MASTER THESIS

Rapid Frequency Offset Mapping with the Half Fourier Acquisition Single-Shot Turbo Spin-Echo with the Selective Parity Approach

Irina De Alba Alvarez

FACULTY OF SCIENCE AND TECHNOLOGY
MASTER IN BIOMEDICAL ENGINEERING
Imaging and in vitro Diagnostics Track

EXAMINATION COMMITTEE

Prof. dr. D.G. Norris
Dr.ir .F.F.J. Simonis
Dr. A. Arbabi

May 2022

UNIVERSITY OF TWENTE.

Rapid Frequency Offset Mapping with the Half Fourier Acquisition Single-Shot Turbo Spin-Echo with the Selective Parity Approach

Irina De Alba Alvarez
Master Thesis in Biomedical Engineering

May 2022

ABSTRACT: Frequency Offset (FO) maps are widely used to correct image distortion and signal loss when magnetic resonance imagine sequences, which are sensitive to field inhomogeneities, are used. The state-of-the-art requires several image acquisitions at different echo times to map the off-resonance frequencies generated by the magnetic field inhomogeneities. This work compares the state-of-the-art method using a modified Half Fourier Acquisition Single-Shot Turbo Spin-Echo (HASTE) sequence with a new proposed method using a Selective Parity (SP) HASTE approach to create FO maps. The SP-HASTE approach needs one single image acquisition followed by image processing to create a frequency offset map. In the experiment different echo times acquisitions were performed to compare the resulting frequency offset maps. Statistical comparison of the results of the SP-HASTE approach and the HASTE were done revealing a comparable agreement between the two methods. They showed a large correlation with values of 1+/-0.05 in the linear regression and not significant frequency differences. The SP-HASTE approach showed a significant reduction in the necessary time to achieve a frequency offset map using one single image acquisition.

KEY WORDS: Frequency offset map; fast spin echo; CPMG; echo parity; magnetic field inhomogeneities; k-space.

1. Introduction

Magnetic resonance imaging (MRI) can suffer from image distortion and signal loss due to the static magnetic field inhomogeneities. This is especially problematic in the case of fast MRI techniques like echo planar imaging with a high sensitivity to the field inhomogeneity of any kind [1]. Therefore, it is important to correct this to avoid the adverse effects of field inhomogeneity and to reduce image distortion and blurring. A conventional method to deal with this problem is through frequency offset (FO) mapping, also known as field mapping [1-3]. A FO map is an image which represents the off-resonance frequencies generated by the magnetic field inhomogeneities across space.

The aim of this work is to propose a method for a rapid FO mapping through only one single acquisition. Two different pulse sequences were used, including half-Fourier acquisition single shot spin-echo (HASTE) and HASTE with the selective parity approach (SP-HASTE). Both methods were based in diffusion weighted (DW) HASTE imaging and were slightly modified to meet the goals of the current work. The HASTE method was used as a reference for the quality evaluation of the results from the proposed approach. First, T_2^* mapping was performed with the HASTE pulse sequence. Then, we performed frequency offset mapping through both methods. Frequency offset mapping with the HASTE method requires several data acquisitions at different time points while increasing an imposed delay time after the excitation radiofrequency (RF) pulse. On the contrary, SP-HASTE enables frequency offset mapping with only one data collection, offering several-folds of time saving

which could be appealing for some applications.

1.1 Magnetic resonance imaging

Magnetic Resonance Imaging (MRI) is a noninvasive imaging technique in which the magnetic property of the tissue can be used to generate images with different types of contrast [4]. In simple words, to create a signal, a strong external magnetic field B_0 is employed to align nuclei with non-zero spins along its direction (z-axes or along the magnet bore). Spins then start precessing around the external magnetic field axes, pointing parallel or anti-Parallel to the B_0 axes. The precessional frequency of the spins is called the Larmor frequency. Then, through a weaker perpendicular magnetic field of B_1, which is generated using radiofrequency pulses, spins are flipped onto the transverse plane (x/y plane), out of their equilibrium. When the RF field is turned off, spins start precessing and going back to their equilibrium through longitudinal relaxation. While the signal is lost the precessional movement of the magnetization induces a small electrical current in the receiver coil. This signal is then processed to turn into an MR image.

1.2 Relaxation mechanisms

Longitudinal or T_1 relaxation is the process by which the net magnetization returns to its initial maximum value after the application of the radio-frequency excitation. In other words, it is the process by which the z component of the magnetization recovers to its initial value. The time it takes for the net magnetization to reach 63% of its maximal value parallel to B_0 is called T_1 relaxation time which depends on the properties of the tissue and is expressed in time units (i.e., milli-seconds).

Transverse or T_2 relaxation is the process by which the transverse component of the magnetization decays due to the spin-to-spin interactions and is irreversible. The time it takes for the transverse magnetization to decay to 37% of its initial value is called the T_2 relaxation time. In the presence of external magnetic field inhomogeneities, magnetization decay is governed by a shorter time constant T_2^*. Signal decay due to the field inhomogeneities is reversible, on the contrary of the T_2 relaxation, with the help of 180° RF refocusing pulses:

$$\frac{1}{T_2'} = \frac{1}{T_2} + \gamma \Delta B_0 \quad [1]$$

where γ is the gyromagnetic ratio constant which is expressed in MHz/Tesla, and ΔB_0 represents the magnetic field inhomogeneities expressed in Tesla.

T_2 and T_2^* relaxation times depend on the properties of the tissue and are expressed in milli-seconds.

1.3 Spatial encoding

To localize the MR signal origin, spatial encoding is performed by means of magnetic field gradients along different axes to encode the frequency and phase of the spins according to their physical position.

Frequency encoding: The main magnetic field is linearly distorted through using a constant amplitude magnetic field gradient during the signal acquisition along the direction of interest, causing the resonance frequency of spins to vary as a function of their position within the slice. Doing this, spins align in this axis will have different resonance frequencies:

$$\omega = \omega_0 + \gamma G_r r \quad [2]$$

where ω is the spatially dependent resonance frequency, ω_0 is the Larmour frequency, γ is the gyromagnetic ratio constant, Gr is the frequency encoding gradient amplitude, and r represents spins' position.

Slice selection: This is accomplished by applying a magnetic field gradient during the

RF pulse along the slice select direction to linearly alter the central resonance frequency of the slices as a function of their position. To select a specific slice, then, the RF pulse's carrying frequency is tuned to the center frequency of the slice of interest. The RF pulse bandwidth and the slice select gradient amplitude will determine the slice thickness.

Phase encoding: This is accomplished by turning on the magnetic field gradient for a limited time in the direction of interest to vary the phase of the spins proportional to their position. Spins in the same row, perpendicular to the gradient, will have the same phase. The generated phase difference for spins in different columns will last until the signal is recorded. When the signal is recorded, a phase rewinder gradient is applied along the same axes with the same amplitude but inverse polarity as the phase encoding gradient to undo the phase differences generated through the previous phase encoding gradient. Although frequency components can easily be differentiated using the Fourier transform in a single echo acquisition, phase differences are not possible. For example, the received signal from voxels A and B would be $A(t) = sin(\omega t + \phi A)$, and $B(t) = sin(\omega t + \phi B)$. The total signal measured in one acquisition would then be $A(t)+B(t)$. The sum of two sines would be $2sin\ [\omega t + ½(\phi A+\phi B)]\ cos\ [½(\phi A - \phi B)]$, where we have the same frequency but an average of the phases. For this reason, it is necessary to alter the amplitude of the phase encoding gradient in a predefined fashion from echo to echo, to traverse the k-space and fill in all the k-space lines.

K-space: The spatially encoded MR signal is collected and used to fill in a frequency domain space called k-space. K-space, in fact, is an array of complex numbers representing the spatial frequencies in the MR image. The k-space center stores the lower frequencies which determine the image gross structure (i.e., contrast). Higher spatial frequencies are stored in the k-space periphery which determine the fine details of the image (i.e., spatial resolution). The inverse Fourier transform of the k-space data would give the MR image.

2. Theory

2.1 Turbo spin-echo

The turbo spin-echo (TSE) or fast spin-echo (FSE) imaging technique has found widespread applications in medical imaging [5]. In this method, as illustrated in figure 1, the net magnetization is initially flipped onto the transverse plane typically using a 90° excitation RF pulse. In other words, it is flipped from the z-axis into the x/y plane.

During evolution time $\tau/2$ (i.e., half of the inter-echo time) after the excitation, spins dephase due to the present local gradients imposed by the external magnetic field inhomogeneities, (i.e., free induction decay due to T_2^* relaxation). Then, a 180° refocusing pulse is employed to rephase the spins and reverse the field inhomogeneities. At the time τ after the excitation, all the spins would be completely rephased, and a spin-echo is formed whose magnitude is governed only by the tissue's T_2 relaxation time. With a proper selection of parameters, including the echo time, this imaging technique can provide images with a T_2-weighted contrast. Echo time is defined as the time from the center of the excitation pulse to the center of the echo used to fill in the central k-space line, which depends on the phase encoding scheme. A series of refocusing RF pulses are usually used to rephase the spins repeatedly to form multiple spin echoes for a faster imaging (Carr-Purcell-Meiboom-Gill (CPMG) train). To do so, the phase encoding gradient's amplitude must be changed from echo to echo to enable sampling of a bunch of k-space lines per excitation. The number of echoes to be formed (i.e., echo train length, ETL), however, is most importantly, limited by the T_2 relaxation time of the

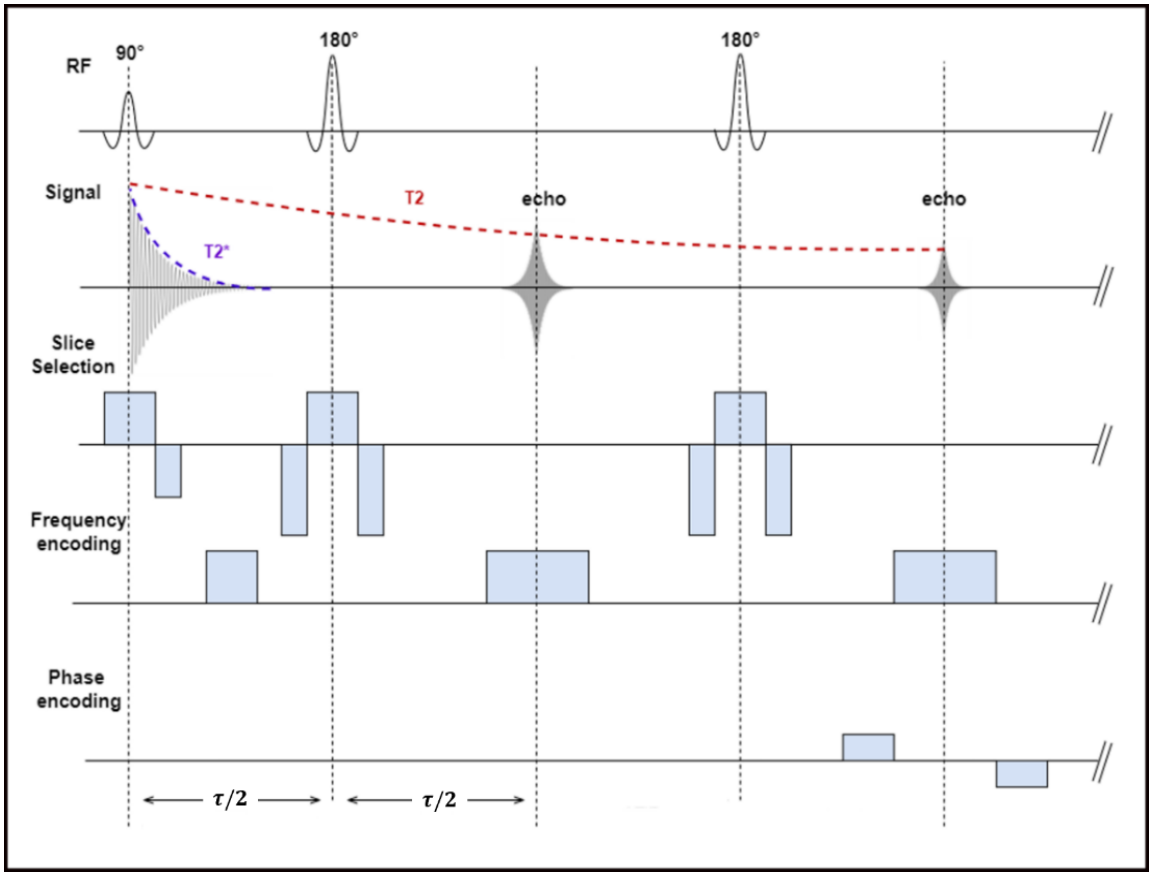

Figure 1. Turbo spin-echo/Fast spin-echo pulse sequence timing diagram: After the 90° excitation RF pulse, a free induction decay signal (FID) is created. Following time $\tau/2$, during which spins dephase and accumulate a phase according to their position, a 180° refocusing RF pulse is employed to reverse the magnetic field inhomogeneities. At the time τ, spins are rephased, and a spin-echo forms. Spatially resolved imaging is accomplished by means of a set of magnetic field gradients to encode the spatial position of spins: (1) Frequency encoding through a fixed amplitude gradient during the echo formation, (2) Phase encoding through variable amplitude gradients to traverse the k-space, and (3) slice selection which is done by means of running slice select gradients during each RF pulse in the direction of interest to excite only a thin slice of the tissue. A train of echoes can be formed by repetitive refocusing the spins for high spatial resolution imaging.

tissue. For high spatial resolution imaging, where a large number of echoes need to be acquired, T_2 relaxation of the tissue could be a limiting factor. To overcome this problem, a multi-shot acquisition can be followed, in which only a sub-section of the k-space is sampled per each excitation pulse. TSE/FSE techniques offer rapid imaging and high signal-to-noise ratio (SNR), while, at the same time, are largely insensitive to static field inhomogeneity artefacts of any kind including magnetic susceptibility and chemical shift artefact due to the presence of 180° refocusing pulses.

The CPMG signal can have contributions from both spin and stimulated echoes in case of inaccurate refocusing RF pulses, or refocusing pulses with a flip angle < 180° (for instance, to decrease their contribution to the specific absorption rate). Assuming a string of 3 RF pulses with an arbitrary flip angle including 1 excitation followed by 2 refocusing RF pulses, a single coherence pathway (i.e., dephasing magnetization) is created after the excitation pulse. This pathway is split into three different pathways by the 1st refocusing RF pulse: (1) a magnetization component which remains unaffected and continues dephasing, (2) a

component which is rephased, and (3) a component which is flipped onto the longitudinal axes [6]. This is repeated for each single pathway that exists at the moment the 2nd refocusing pulse is applied. When pathways cross the horizontal axis (i.e. the midway axes between the RF pulses), a spin echo or a stimulated echo forms. Even a small number of such refocusing pulses can lead to the formation of a large number of pathways. The echoes formed by pathways in which the magnetization has spent an odd number of refocusing pulses are referred to as odd echo parities, and even parity echoes form analogously [7]. The 2 echo families have a relative intensity determined by the flip angle of the refocusing pulses. If the flip angle of the refocusing pulse is exactly 180°, only pure Hahn spin echoes will be generated. This means that the 2 echo families will happen at the same time and will contribute positively to each other.

The phase of the spin echo depends on the phase of the refocusing RF pulse. For example, assuming the excitation pulse is applied along the +x-axis, the transverse magnetization will be aligned in the +y direction. Then, with the application of the refocusing pulse of 180° along the +x-axis, the spins will rotate around the +x-axis, and eventually form in the -y direction (figure 2). On the other hand, if the refocusing pulse is applied in the +y-axis, spins will rotate around the +y-axis and the echo will form in the +y-direction (figure 3).

2.2 CPMG/non-CPMG condition

In techniques using the CPMG readout for the rapid data collection, like TSE/FSE pulse sequence, a so-called CPMG condition must be met. This is not possible unless there exists a 90° phase difference between the excitation and refocusing RF pulses [8] (i.e., refocusing RF pulse must be parallel or anti-parallel to the transverse magnetization).

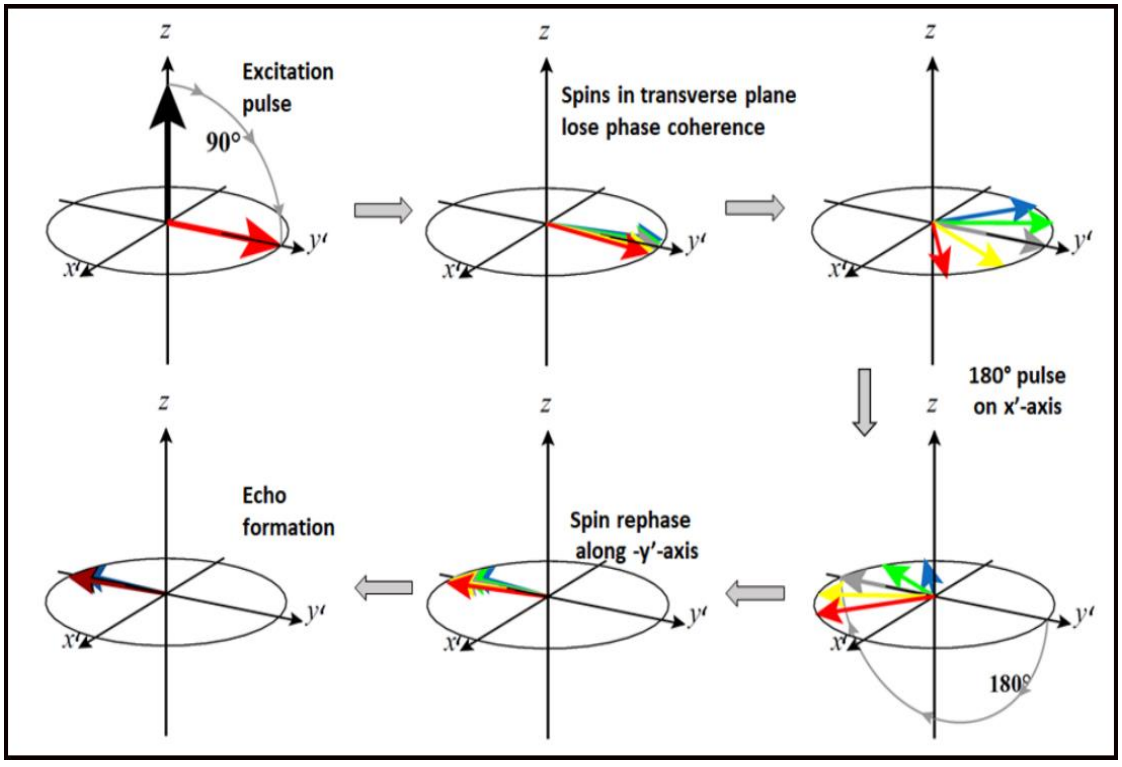

Figure 2. Spin-echo formation (non-CPMG condition): Excitation and refocusing RF pulses are applied while having the same phase; the spin-echo is formed in -y-axis.

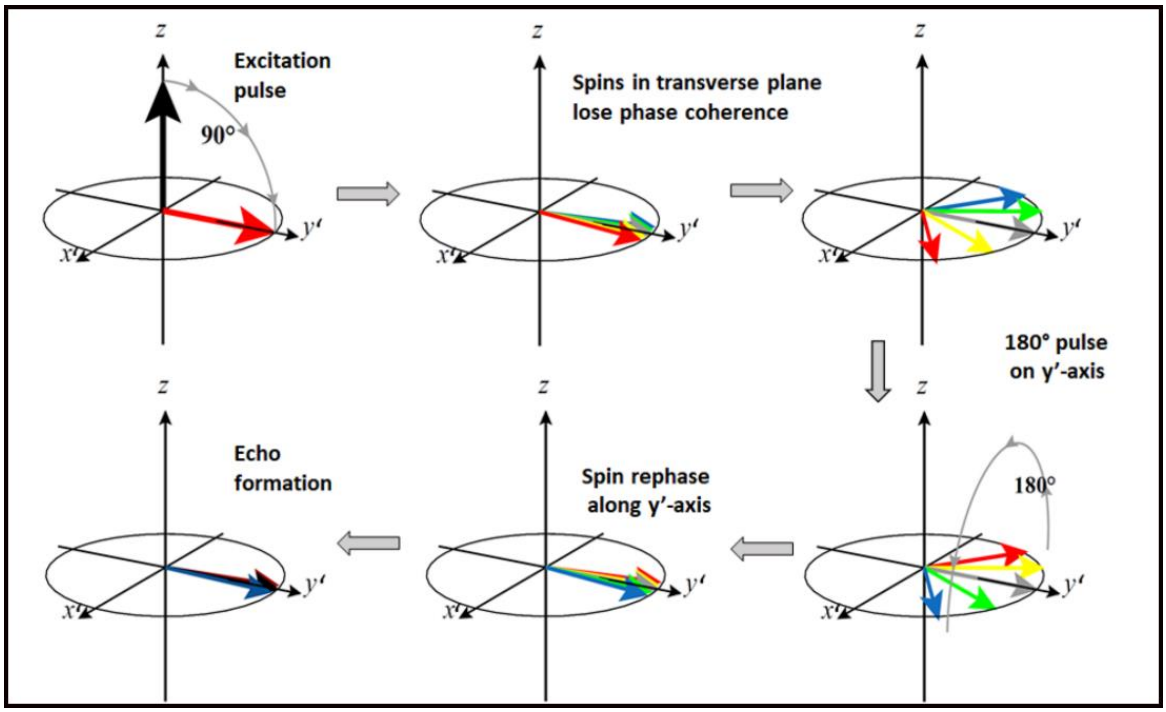

Figure 3. Spin-echo formation (CPMG condition): Excitation RF pulse is aligned along the +x-axis, and the refocusing RF pulse is perpendicular to the excitation pulse (i.e., applied along the +y-axis), and parallel to the transverse magnetization. The echo is formed along the +y-axis.

In certain situations, the CPMG condition can be violated (i.e., non-CPMG), and, as a result, the echoes with the odd and even parities would destructively interfere resulting in irremediable consequences for the image quality.

In three specific situations the CPMG condition can be violated: (1) T_2^* imaging [7-9, 10] and (2) spectroscopic imaging, where an additional evolution period is introduced between the excitation pulse and the first refocusing pulse [11], and (3) Diffusion-weighted imaging (DWI) [12], where any bulk motion during the strong diffusion encoding gradients can lead to an unknown arbitrary phase shift between the echo parities.

A few solutions for the non-CPMG problem have been proposed in the literature. One of the oldest methods to resolve this problem is to acquire only one of the echo parities and ignore the other one [7]. In this approach, the echo parity of interest is selected at each echo time while the other parity is moved out of the acquisition window by means of a displacing gradient implemented either before (to select the even parity echo) or after (to select the odd parity echo) the read-out gradient. Notable drawbacks of this method include smaller SNR due to the loss of sensitivity, and a need for dummy cycles before the acquisition to stabilize the amplitude of early echoes, which unnecessarily increases the echo time leading to a loss of signal. Another proposed method to tackle this problem, which does not require the implementation of displacing gradients, is to acquire both echo parities in split acquisition windows [13-14]. However, it also suffers from the decay of signal due to T_2 and is limited to low resolution imaging. The selective parity approach, as a novel technique, offers some solutions to these limitations which will be discussed later in section 2.5.

2.3 *Half-Fourier acquisition single shot turbo spin echo*

Half-Fourier acquisition single shot turbo spin-echo (HASTE) is a variant of the TSE/FSE method in which a little more than one-half of the k-space is sampled following only one single excitation, and the remaining lines are estimated through partial Fourier method using the phase conjugate symmetry of the k-space during the reconstruction [15].

2.4 *Modified HASTE pulse sequence*

Diffusion weighted HASTE (DW-HASTE) pulse sequence is a HASTE-based method which is used for diffusion-weighted magnetic resonance imaging. The original Siemens's DW-HASTE pulse was modified for spatially resolved T_2* and FO mapping. To do so, a variable delay time was implemented between the 90° excitation and the first 180° refocusing RF pulses, and the diffusion encoding preparation module was removed, for this reason it is called just HASTE in the rest of the article. To avoid artifacts arisen from the non-CPMG condition due to the evolution of spins during the delay time, a displacing gradient was used prior to each read-out gradient to remove the odd parity echo out of the acquisition window and acquire only the even parity echo at each echo time (figure 4). Four dummy cycles were also used at the start of the acquisition to wait for stabilization of the early echo amplitudes.

2.5 *HASTE with a selective parity approach*

As explained in section 2.2, available solutions for the non-CPMG problem come with certain limitations. The selective parity approach, initially introduced in [14], offers solutions to these limitations and provides nearly full sensitivity through benefiting from both echo parities in t0h0000000e image formation, while providing the same image quality.

In this study, we used a more developed version of the SP-HASTE method [16]. For the experiments performed in this work, the pulse sequence was, slightly modified through implementing a variable delay time between the excitation and first refocusing RF pulse and removing the diffusion encoding preparation

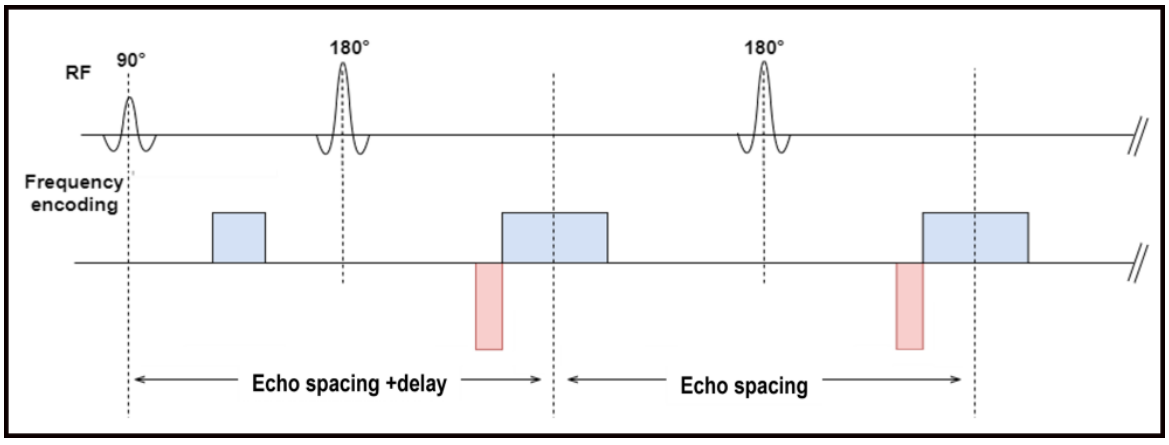

Figure 4. The timing diagram of the modified HASTE pulse sequence: A variable delay time was implemented between the excitation and the first refocusing RF pulses. The diffusion encoding preparation module was also removed. Displacing gradients, as depicted by red boxes, were used before each read-out gradient to acquire only even parity echoes and avoid image distortion due to the non-CPMG condition. Only the RF pulse train and frequency encoding direction are shown for the first 2 echoes.

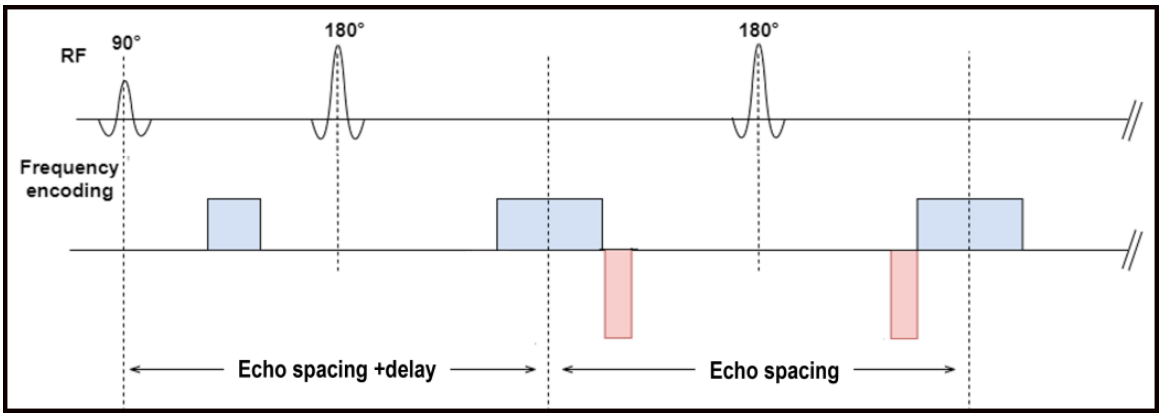

Figure 5. The timing diagram of the modified SP-HASTE pulse sequence: A variable delay time was implemented between the excitation and the first refocusing RF pulses. The diffusion encoding preparation module was removed. Displacing gradients, as depicted by red boxes, were used either before (to select even parity echoes) or after (to select odd echo parities) at each echo time. Only the RF pulse train and frequency encoding direction are shown for the first 2 echoes. RF pulse waveforms shown do not represent the SLR refocusing RF pulses used in the method.

module. This method, in fact, is a variant of the HASTE pulse sequence in which displacement gradients are employed either before or after the read-out gradient to acquire the echo parities in an alternating fashion (figure 5).

Shinar Le-Roux (SLR) [17] refocusing RF pulses are employed for their better slice profiles resulting in a smooth signal intensity decay over early echoes. This makes the use of dummy cycles for the echo amplitude stabilization unnecessary which leads to a shorter TE and higher signal intensity, compared to the manufacturer's original HASTE pulse sequence. Better slice profiles of the SLR RF pulses come at the cost of a higher specific absorption rate (SAR) contribution

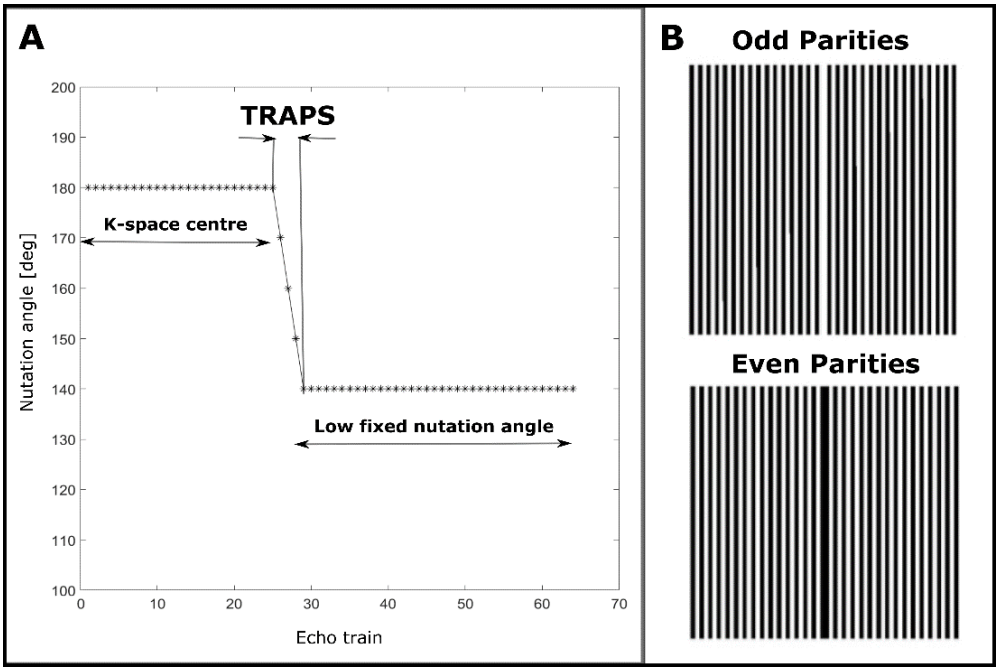

Figure 6. SP-HASTE: (A) TRAPS to reduce the SAR contribution from SLR refocusing pulses. The k-space center is sampled using nominally 180° pulses, and then, the nutation angle is reduced to a fixed low flip angle. (B) The center-out phase encoding scheme to sample the k-space while alternating echo parities,

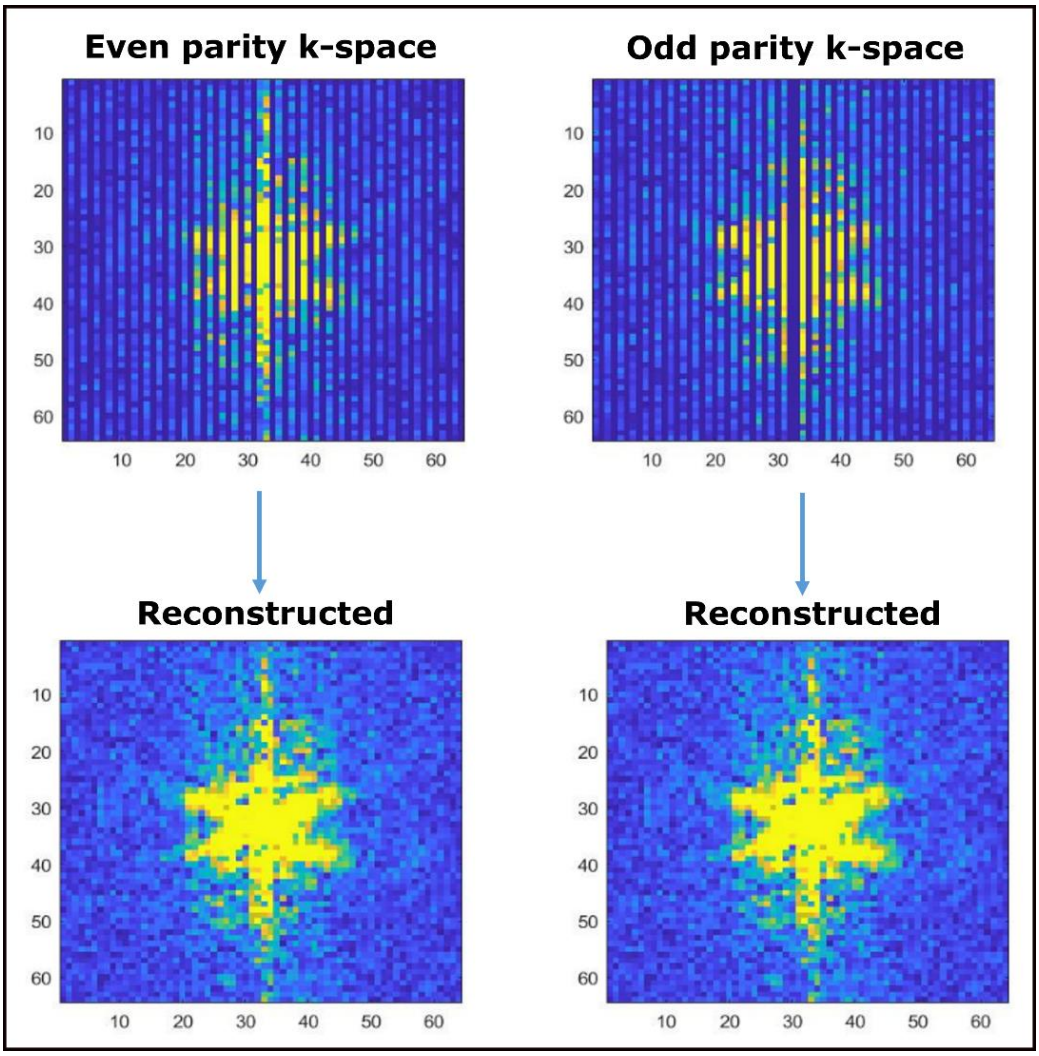

Figure 7. Even and odd echo parity k-spaces created in the reconstruction: Undersampled lines can be seen in the original k-spaces (top row). Bottom row shows the same k-spaces with the missing lines estimated through the SPIRiT algorithm (bottom row).

which is compensated for with smooth transition between pseudo steady states (TRAPS [18], figure 6A). A center-out phase encoding scheme is also employed to sample the k-space with evenly distributed odd and even echo parities (figure 6B).

In the reconstruction [16], acquired echo parities are used to create 2 separate k-spaces (figure 7). The odd and even k-space missing lines are then estimated through SPIRiT (GRAPPA) algorithm [19]. An iterative process is later used to ensure the odd and even parities are complex conjugates of each other in the image domain considering the CPMG angle as the frame of reference. This iterative approach converges to a consistent representation of the non-acquired data lines without additional G-noise and is depicted in figure 8.

The critical step is the estimation of the CPMG phase map (step 3), which is subsequently used to convert odd parity to even parity data and vice versa (step 4). The information from both echo parities is then combined in step 5. After ~30 iterations (relative error below 1%), odd parity and even parity images eventually converge to the same solution, providing identical magnitude images.

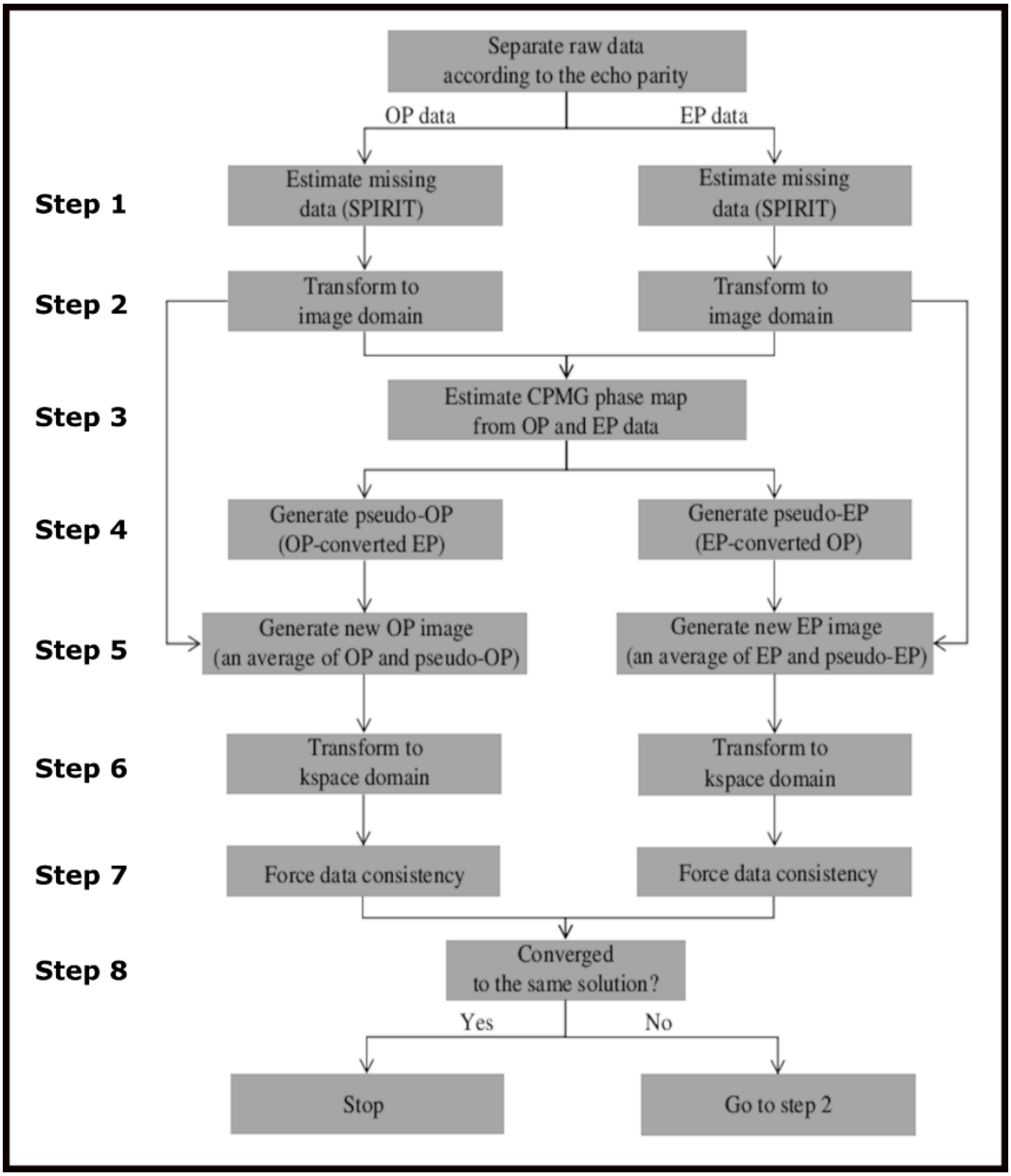

Figure 8. Schematic of the SP-HASTE reconstruction.

2.6 Frequency offset mapping

A Frequency offset (FO) map, also known as local field map, is a spatially resolved image generated from the unwanted phases accumulated by spins during an evolution time due to the local magnetic field inhomogeneities and is usually expressed in the unit of Hz. In fact, it shows spins' local resonance frequency deviation from the reference Larmor frequency. The easiest way to calculate a FO map is through acquiring images with 2 different TE's using a pulse sequence sensitive to the magnetic field inhomogeneities. Looking into the phase difference of the acquired images with respect

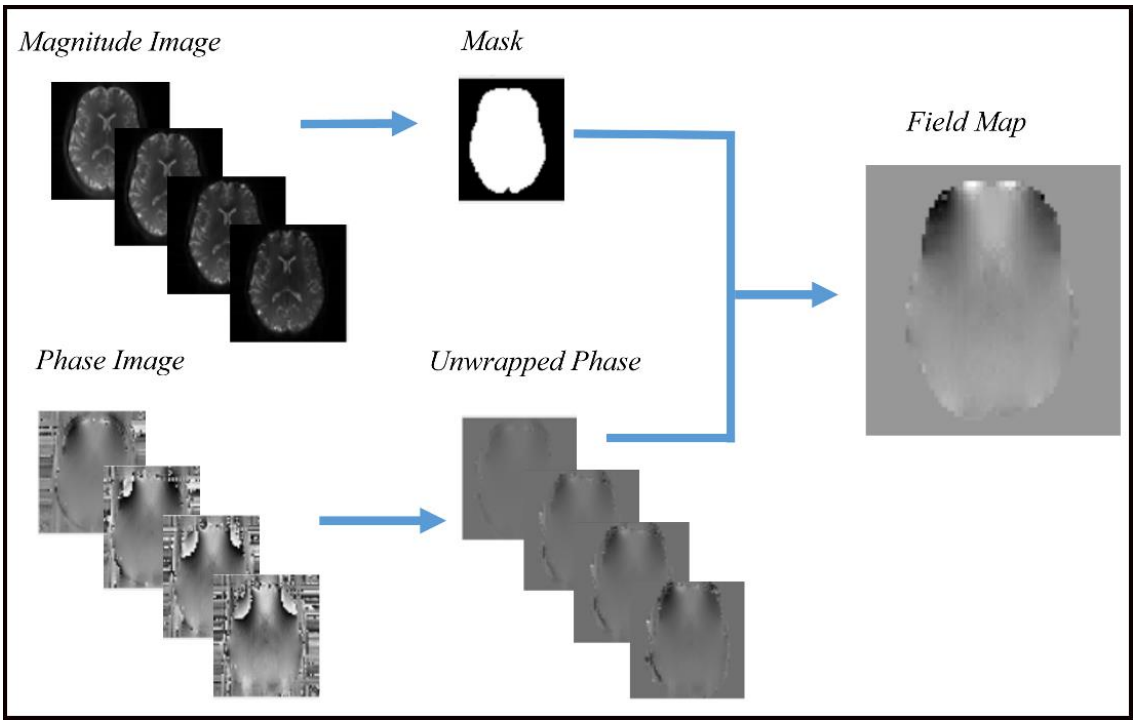

Figure 9. The schematic of the frequency offset mapping: Multiple acquisitions with different TE's are performed. Magnitude images are used to create a mask to be used for the background noise removal. Phase images are then calculated, unwrapped, and masked. Finally, the frequency offset within each voxel is calculated by finding the slope of the phase versus time graph for each voxel.

to their time point difference for each voxel, a spatially resolved FO map can be created:

$$FO = \frac{P_2 - P_1}{TE_2 - TE_1} \quad [3]$$

where p_1 and p_2 are the accumulated phases by spins within each voxel and TE_1 and TE_2 are the echo times of the acquired images.

A more precise and routine approach, however, is to acquire several images at different time points (i.e., different TE's), and then calculate the slope of the phase versus time for each voxel.

Figure 9 illustrates the main steps involved in the FO mapping. Several acquisitions with different TE's are performed. Magnitude images are used to produce a proper mask. The produced mask can be used to remove the background noise. Phase images are then calculated and unwrapped to find the proper phase angle within each voxel. Finally, frequency offset within each voxel is calculated through finding the slope of the phase versus time graph for each voxel.

3. Methods

MRI scans were performed on a whole body 3T Siemens Prisma/PrismaFit scanner (80 mT/m strength and 200 mT/m/ms slew rate) with a 32-channel receive-only head coil in 1 healthy female volunteer. Common parameters were as follows: TR = 2000 ms , FOV= 200 * 200 mm, matrix size of 64*64, 3.1 mm isotropic in-plane resolution, 3 axially oriented slices (3 mm), and 20 repetitions. No accelerated imaging was used for the data collection. Data were collected with delay times ranging from 0 to 42 ms with the increments of 6ms. TE and echo spacing were 50 ms and 7.34 ms for the modified HASTE and 13 ms and 7.09 ms for the modified SP-HASTE, respectively.

4. Results

Figure 10 shows the magnitude images obtained with the modified HASTE method for different delay times.

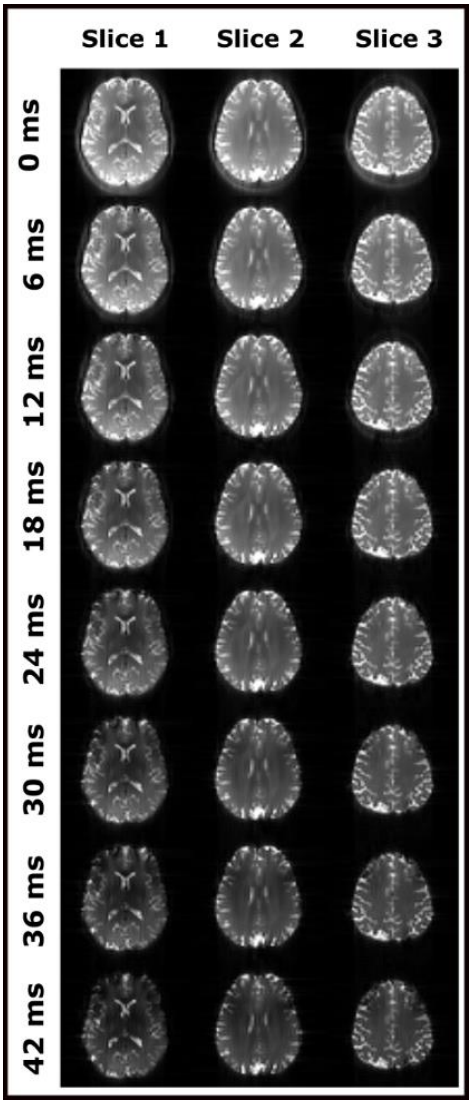

Figure 10. Example axial T_{2}^{*}-weighted slices from the modified HASTE pulse sequence in a healthy female volunteer at 3T: From left to right, 3 sample slices, and from top to bottom, images corresponding to each delay time are presented. A signal drop is visible with the increasing delay time. Less signal drop from the cerebrospinal fluid (CSF) is perceived due to its long T_2^* relaxation time. A faster signal drop is also observed for white matter compared to grey matter. The background noise has been masked.

A mono-exponential fitting routine was performed pixel-wise through the magnitude images obtained with the modified HASTE to create spatially resolved T_{2}^{*} maps (equation [4]).

$$S = A \cdot exp\ (-t/T_2^*) \qquad [4]$$

where *t* represents the delay time, *S* is the signal value within each voxel, and *A* and T_{2}^{*} are the variables to be estimated. With the estimated values of T_{2}^{*} of each voxel we can create a map to see the differences about our signal decay due to magnetic field inhomogeneities.

Estimated T_2^* maps are presented in figure 11 for the same sample slices shown in Figure 10.

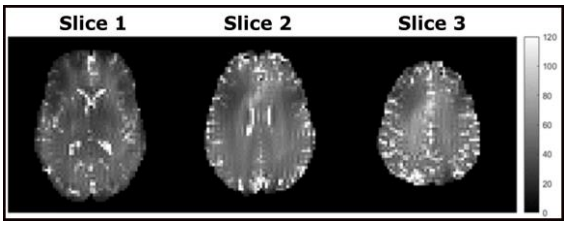

Figure 11. Estimated T_2^* maps for the same slices as shown in figure 10: Values are expressed in ms. The background noise has been masked.

For FO mapping, SEPIA, a Quantitative Susceptibility Map (QSM) software [20] was used to unwrap the phases for the acquired 20 repetitions and 8 delay times to continue with the field map calculation. For the modified SP-HASTE sequence, the 0ms delay time was disregarded since no phase shift is generated between the odd and even parity echoes. Nevertheless, for the modified SP-HASTE method, only one acquisition was enough to generate the FO maps using equation [5]:

$$FO = \frac{P_{even} - P_{odd}}{t} \qquad [5]$$

where P_{odd} and P_{even} are the odd and even parity phase images, respectively, and t is the delay time.

Figure 12 presents the FO maps created with the modified HASTE sequence. FO maps created with the modified SP-HASTE method for each delay time are shown in figure 13.

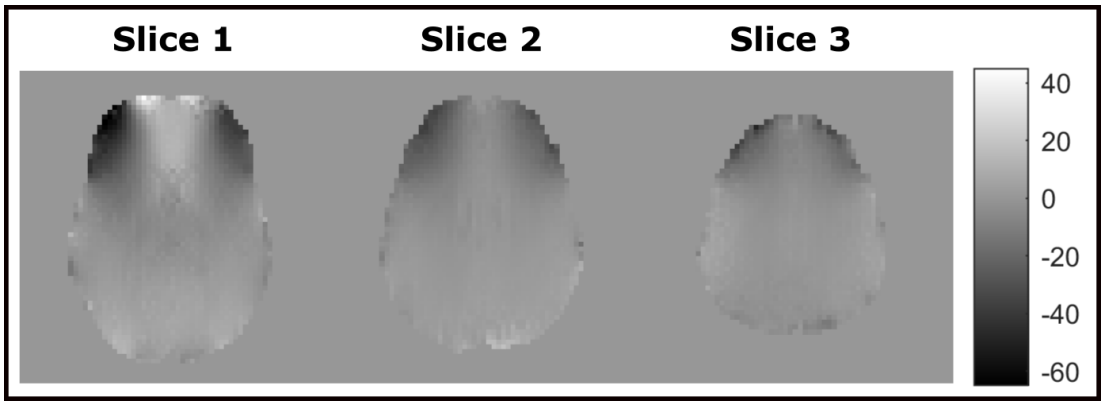

Figure 12. FO maps created with the modified HASTE sequence: From left to right, the same slices as in figure 10 are shown. Units are expressed in Hz.

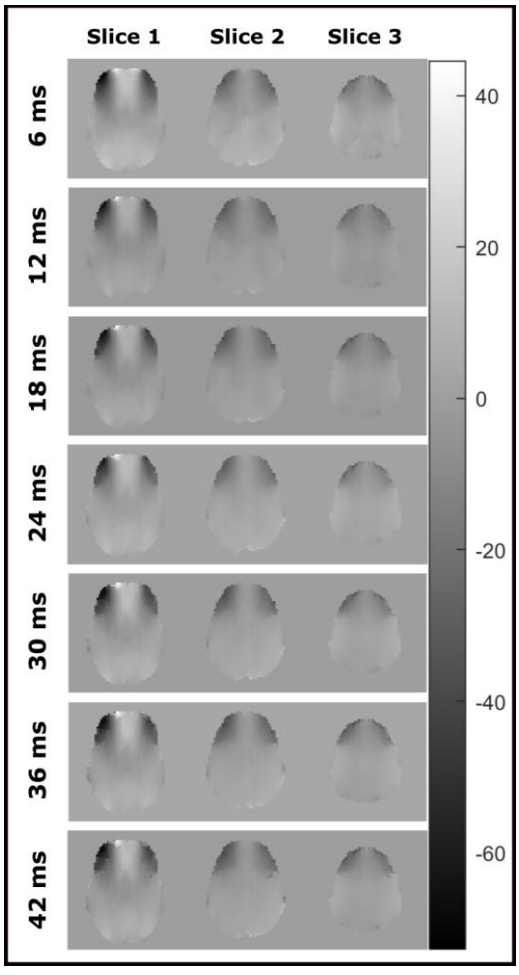

Figure 13. FO maps created with the modified SP-HASTE sequence from different delay times: From left to right, the same slices as in figure 10, and, from top to bottom, FO maps corresponding to each delay time are presented. Units are expressed in Hz.

A linear regression was performed for the FO mean values obtained with the modified SP-HASTE for all delay times versus the FO mean value from the modified HASTE method. This was done to identify the relationship between the two FO results. To do so, the HASTE FO mean value was treated as the ground truth A and the SP-HASTE FO mean values as B, and slope and intercepts of a predicted line were estimated:

$$f = b + mA \quad [6]$$

where b is the intercept and m represents the regression slope.

In general, the predicted regression slope of 1±0.05 shows a very good agreement between the 2 methods for slice 1 (table 1). Although no meaningful difference is found among different delay times, the highest and lowest linear correlation is observed for 12 ms and 30 ms delay times, respectively, between the 2 methods. A decreasing linear correlation can be seen, however, for FO > 25 HZ between the methods in figure 14.

Delay Times [ms]	6	12	18	24	30	36	42
Slope	0.9497	0.9912	1.0321	1.0447	1.0522	1.0327	1.0246

Table 1. The predicted linear regression slope for slice 1: Linear regression was performed for the FO mean values obtained with the modified SP-HASTE for delay times ranging from 6 to 42 ms versus the FO

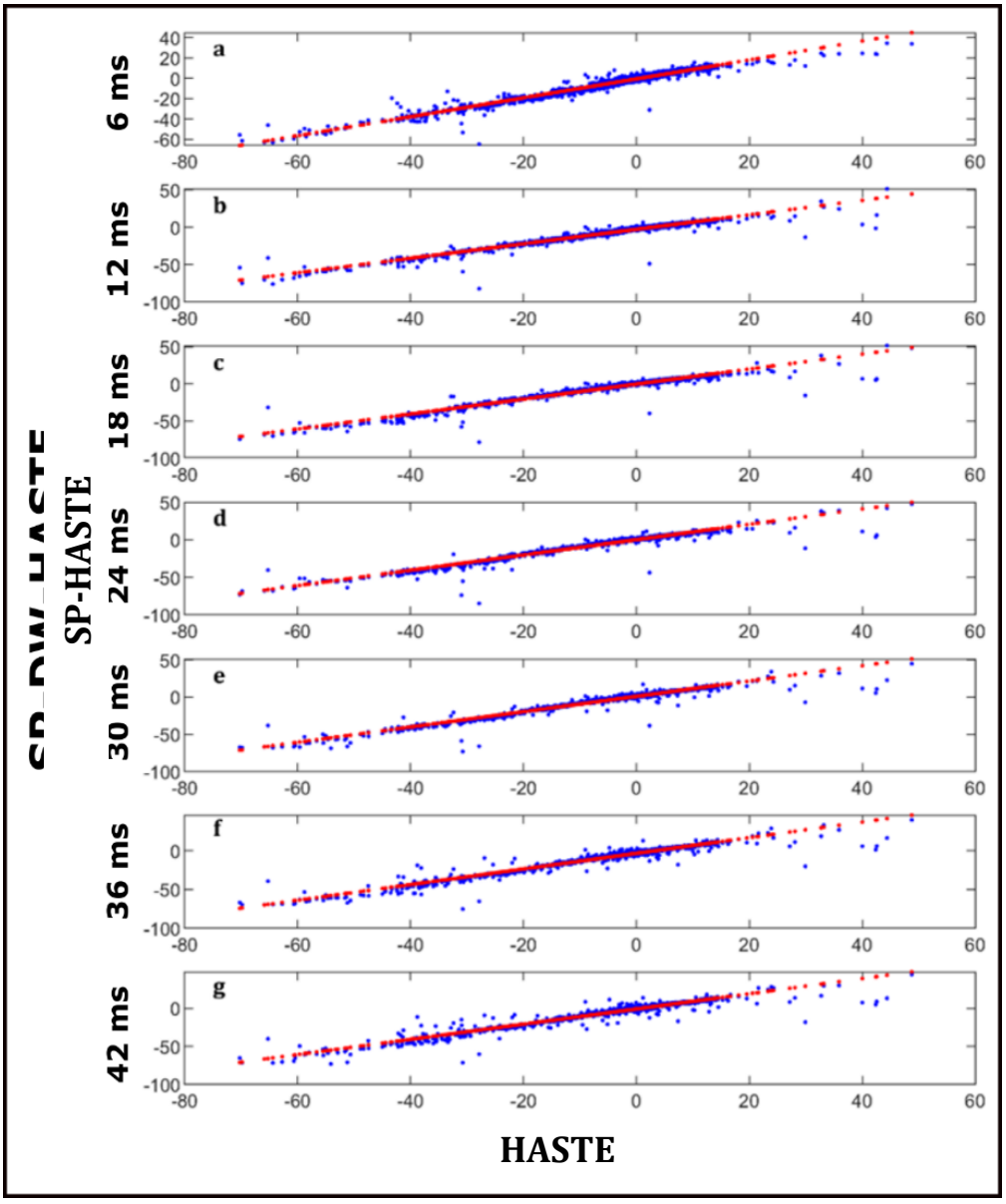

Figure 14. Linear regression of the FO values obtained with the modified SP-HASTE versus those obtained with the modified HASTE for slice 1 for different delay times. The red line on each panel represents the predicted slope.

The standard deviation (Std) was used as a measure of the image time course dispersion (noise). The temporal Std was calculated over 20 acquired repetitions using equation [7], for the FO maps obtained with both methods. For the modified SP-HASTE FO maps, the process was repeated for all the delay times (6-42 ms).

$$\sigma = \sqrt{\frac{\sum_{i=1}^{N} |A_i - \mu|^2}{N-1}} \qquad [7]$$

where μ is the mean FO value of the 20 repetitions, N is the number of repetitions (20), and A represents the FO value within each voxel.

Calculated Std maps are presented in figure 15 for the FO maps obtained with the modified HASTE and SP-HASTE. Overall, a good agreement can be seen between the 2 methods. Slightly higher Std values are observable for the modified SP-HASTE FO maps obtained from 6 and 24 ms delay times which reflect more fluctuation between the measurements for these delay times.

Figure 16 illustrates the difference between the FO values estimated with the 2 methods for all the delay times for slice 1. The smallest median difference was found for 6 ms and 18ms delay times, with the FO difference close to 0 Hz. The biggest median difference was for 36ms delay time with a median difference of 2.62Hz. The delay times which showed the narrowest whiskers were 18ms and 42ms.

5. Discussion

The linear regression showed a good linear correlation between the results from the SP-HASTE and HASTE methods for all the delay times with the slope of 1±0.05. Bigger errors observed for the estimated FO values > 25 Hz could be due to the phase unwrapping errors originated from SEPIA (see Fig. 14). We believe this is due to the high phase wrapping rate that occurred mainly in the front part of the brain (i. e., frontal lobe) in slice 1. This error did not occur in slice 2 and 3, and they did not present that high phase wrapping either.

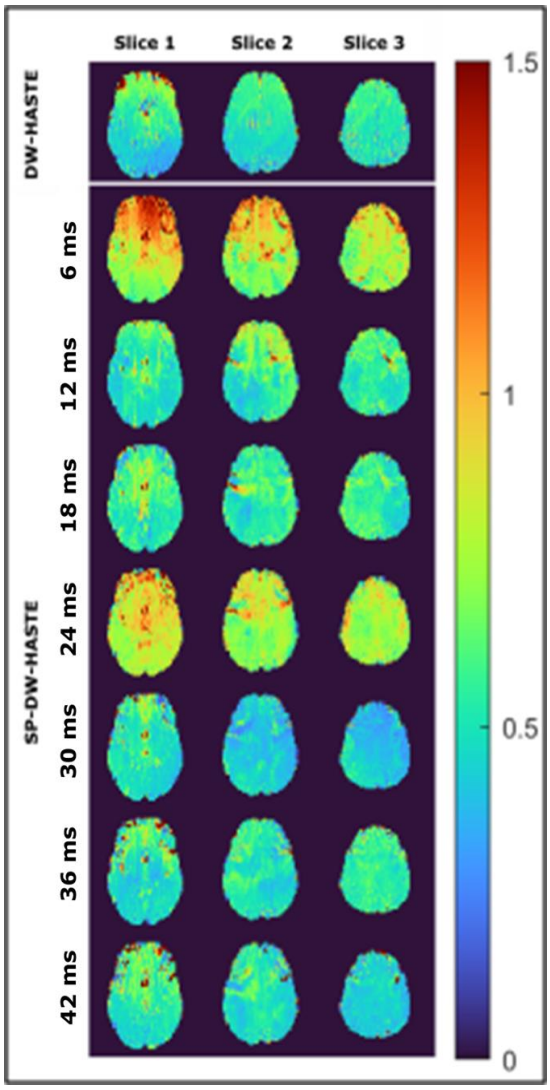

Figure 15. Temporal standard deviation maps calculated over 20 repetitions for the FO values obtained with the proposed methods for different delay times: The SP-HASTE FO maps obtained with 6 and 24 ms delay times show a higher Std compared to the HASTE method. The SP- HASTE FO map estimated for 30 ms delay time has smaller Std compared to the HASTE method for slices 2 and 3. A comparable agreement can be observed between the 2 methods for the other delay times.

The Std analysis worked as an evaluation of the quality of our measurements. The slightly higher Std values for 6ms and 24ms delay times for the SP-HASTE method could be due to some subject movements between the acquisition repetitions, because there is not a congruent explanation to have just two of the delay sequences to present more noise than the

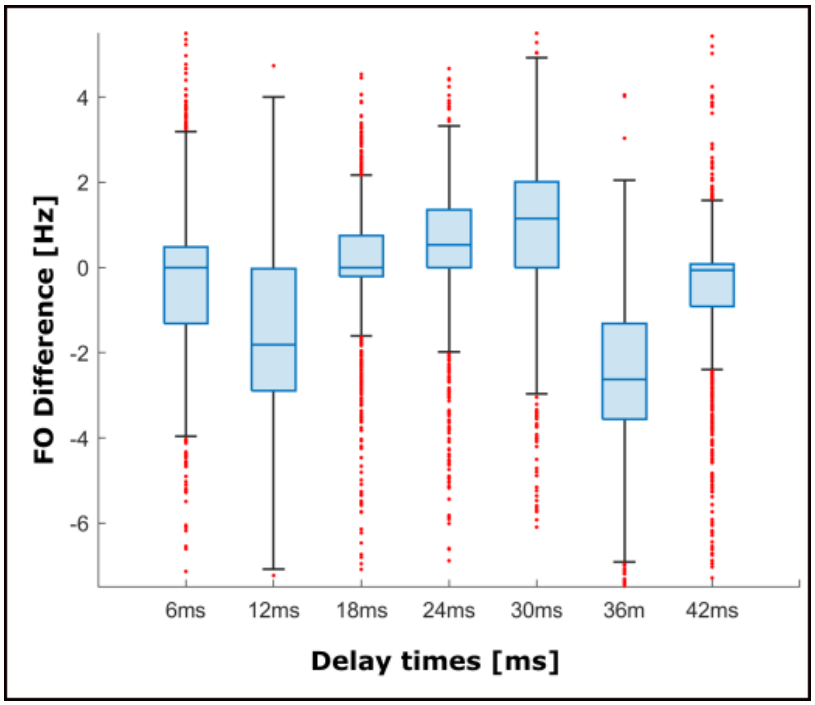

Figure 16. Box plot of the difference between the FO values estimated using the modified SP-HASTE and HASTE for slice 1 as shown in figure 11 for all the delay times.

others in those time intervals. A solution for this could be to explain the subject to stay very still.

FO difference calculations for slice 1 between the 2 methods revealed the closest results for 18 ms and 42ms delay times with the median close to 0 Hz and quartiles difference of about 1 Hz (0.9 Hz for 18ms and 1.0141 Hz for 42ms). Our analysis for slices 2 and 3 revealed comparable results, which can be found in Appendix A.

The SP-HASTE pulse sequence used in this research was in-house work, which means that it is currently being developed and it is not a commercial sequence used in other laboratories or hospitals. We were limited to imaging with a low spatial resolution. Higher spatial resolution imaging would require acquiring a higher number of echoes, which was not feasible , due to the artefacts arising from the T_2 blurring of the k-space (i.e., echo train length > T_2 relaxation of the brain tissue).

Achieving higher spatial resolution through increasing the acceleration factor of imagine was also not possible at the time we were undergoing our measurements for the SP-HASTE sequence. This was because using an acceleration factor of at least 2 for a complete k-space would lead to an acceleration factor of 4 in the individual even and odd k-spaces, which could not be handled by the under the development reconstruction program due to the high number of undersampled lines.

6. Conclusion

In this work, we performed frequency offset mapping through 2 variants of the Siemens HASTE pulse sequence at 3T. To do so, HASTE and SP-HASTE pulse sequences were modified by removing the diffusion encoding preparation module and implementing a variable delay time between the excitation and first refocusing RF pulse. We

also did T_2^* mapping with the modified HASTE method.

The SP-HASTE method, as a novel approach, enables frequency offset mapping with the acquisition of one dataset from a single delay time, while HASTE method requires several datasets to be collected for a range of delay times. The linear regression analysis performed on the estimated frequency offset maps, among all other statistical analyses performed, demonstrated a comparable agreement between the 2 methods. The several-folds of time saving offered by the SP-HASTE method could find applications in research like assessment of fast changing magnitudes.

7. Acknowledgments

The author gratefully acknowledges the considerable help given by Prof. David Norris and Dr. Aidin Arbabi for they assistance and comments on the manuscript as well as they supervision during the project, the MRI techniques group of the Donders Institute for Brain, Cognition and Behavior, to Dr. J. P. Marques and Kwok-Shing Chan for their help with SEPIA, to Dr. V. Khlebnikov for his help in the SP-HASTE image reconstruction program and to Dr. Frank Simonis for his supervision and comments done in the manuscript.

Together, we can do anything.

-Norbury, James, *"Big Panda and Tiny Dragon"*

8. References

[1] J. J. Riera *et al.*, "Effects of Field-Map Distortion Correction on Resting State Functional Connectivity MRI," *Frontiers in Neuroscience | www.frontiersin.org*, vol. 11, p. 656, 2017, doi: 10.3389/fnins.2017.00656.

[2] R. Cusack, M. Brett, and K. Osswald, "An Evaluation of the Use of Magnetic Field Maps to Undistort Echo-Planar Images," *Neuroimage*, vol. 18, no. 1, pp. 127–142, Jan. 2003, doi: 10.1006/NIMG.2002.1281.

[3] P. Jezzard and R. S. Balaban, "Correction for geometric distortion in echo planar images from B0 field variations," *Magnetic Resonance in Medicine*, vol. 34, no. 1, pp. 65–73, 1995, doi: https://doi.org/10.1002/mrm.1910340111.

[4] W. R. Hendee and C. J. Morgan, "e ProgrXes st Magnetic Resonance Imaging Part I-Physical Principles".

[5] B. Kiefer, "Turbo Spin-Echo Imaging," in *Echo-Planar Imaging: Theory, Technique and Application*, Berlin, Heidelberg: Springer Berlin Heidelberg, 1998, pp. 583–604. doi: 10.1007/978-3-642-80443-4_19.

[6] Norris, D. G., & Börnert, P. (1993). Coherence and Interference in Ultrafast RARE Experiments. *Journal of Magnetic Resonance, Series A*, *105*(2), 123–127. https://doi.org/10.1006/JMRA.1993.1263

[7] D. G. Norris, P. Börnert, T. Reese, and D. Leibfritz, "On the application of ultra-fast rare experiments," *Magnetic Resonance in Medicine*, vol. 27, no. 1,

pp. 142–164, 1992, doi: https://doi.org/10.1002/mrm.1910270114.

[8] H. Y. Carr and E. M. Purcell, "Effects of Diffusion on Free Precession in Nuclear Magnetic Resonance Experiments," *Physical Review*, vol. 94, no. 3, pp. 630–638, May 1954, doi: 10.1103/PhysRev.94.630.

[9] D. G. Norris, M. Hoehn-Berlage, F. Wittlich, T. Back, and D. Leibfritz, "Dynamic imaging with T2∗ contrast using U-FLARE," *Magnetic Resonance Imaging*, vol. 11, no. 7, pp. 921–924, Jan. 1993, doi: 10.1016/0730-725X(93)90210-5.

[10] T. Niendorf, "On the application of susceptibility-weighted ultra-fast low-angle RARE experiments in functional MR imaging," *Magnetic Resonance in Medicine*, vol. 41, no. 6, pp. 1189–1198, Jun. 1999, doi: https://doi.org/10.1002/(SICI)1522-2594(199906)41:6<1189::AID-MRM15>3.0.CO;2-1.

[11] D. G. Norris and W. Dreher, "Fast proton spectroscopic imaging using the sliced k-space method," *Magnetic Resonance in Medicine*, vol. 30, no. 5, pp. 641–645, Nov. 1993, doi: https://doi.org/10.1002/mrm.1910300516.

[12] D. G. Norris and T. Niendorf, "Interpretation of DW-NMR data: Dependence on experimental conditions," *NMR in Biomedicine*, vol. 8, no. 7, pp. 280–288, Nov. 1995, doi: https://doi.org/10.1002/nbm.1940080703.

[13] F. Schick, "SPLICE: Sub-Second Diffusion-Sensitive MR Imaging Using a Modified Fast Spin-Echo Acquisition Mode," 1997.

[14] D. G. Norris, "Selective parity RARE imaging," *Magnetic Resonance in Medicine*, vol. 58, no. 4, pp. 643–649, 2007, doi: 10.1002/mrm.21339.

[15] M. R. Patel, R. A. Klufas, R. A. Alberico, and R. R. Edelman, "Half-Fourier Acquisition Single-Shot Turbo Spin-Echo (HASTE) MR: Comparison with Fast Spin-Echo MR in Diseases of the Brain," 1997.

[16] A. Arbabi, V. Khlebnikov, J. P. Marques, and D. G. Norris, "Robust and Motion-Insensitive Approach to Diffusion-Weighted Half-Fourier Acquisition Single-Shot Turbo Spin-Echo Imaging," 2022.

[17] P. le Roux, "Non-CPMG Fast Spin Echo with Full Signal," *Journal of Magnetic Resonance*, vol. 155, no. 2, pp. 278–292, Apr. 2002, doi: 10.1006/JMRE.2002.2523.

[18] J. Hennig, M. Weigel, and K. Scheffler, "Multiecho sequences with variable refocusing flip angles: Optimization of signal behavior using smooth transitions between pseudo steady states (TRAPS)," *Magnetic Resonance in Medicine*, vol. 49, no. 3, pp. 527–535, 2003, doi: https://doi.org/10.1002/mrm.10391.

[19] M. Lustig and J. M. Pauly, "SPIRiT: Iterative Self-consistent Parallel Imaging Reconstruction From Arbitrary k-Space," *Magnetic Resonance in Medicine*, vol. 64, pp. 457–471, 2010, doi: 10.1002/mrm.22428.

[20] K. S. Chan and J. P. Marques, "SEPIA—Susceptibility mapping pipeline tool for phase images," *Neuroimage*, vol. 227, p. 117611, Feb. 2021, doi: 10.1016/J.NEUROIMAGE.2020.117611.

8. Appendix A

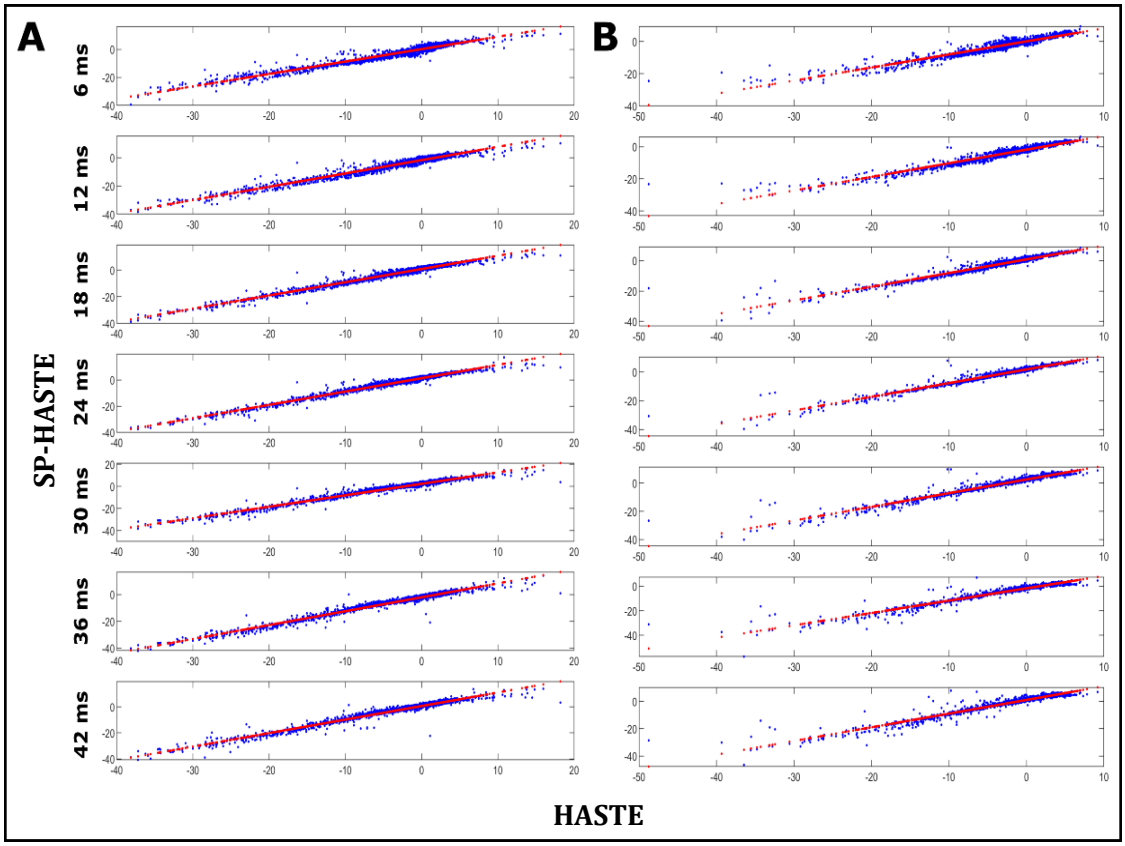

Figure 1. Linear regression of the FO values obtained with the modified SP-HASTE versus those obtained with the modified HASTE for: (A) slice 2 and (B) slice 3 as shown in figure 11 for different delay times. The red line on each panel represents the predicted slope.

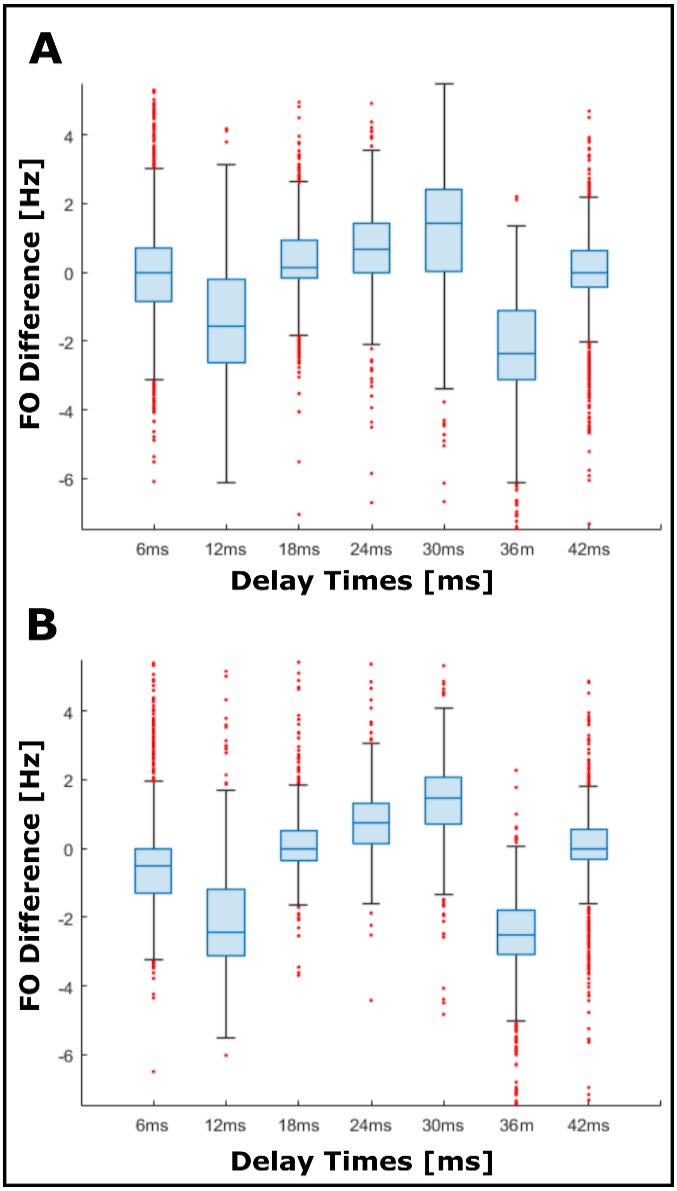

Figure 2. The box plot of the difference between the FO values estimated using the modified SP-HASTE and HASTE for: (A) slice 2 and (B) slice 3 as shown in figure 11 for different delay times.